

GRADIENT-BASED OPTIMIZATION OF A 3D TURBINE VANE FRAME

L. Zampini^{1,2} - L. Mueller¹ - S. Lavagnoli¹ - G. Coussement² - T. Verstraete¹

¹Turbomachine and Propulsion Department, von Karman Institute, Belgium

²Fluids-Machines Unit, Faculty of Engineering, University of Mons, Belgium
luca.zampini@vki.ac.be - lasse.mueller@vki.ac.be - sergio.lavagnoli@vki.ac.be -
gregory.coussement@umons.ac.be - tom.verstraete@vki.ac.be

ABSTRACT

The trend towards increased by-pass ratio has implied a significant growth in the radial extension of every component in modern aero engines. This has made the design of the Turbine Vane Frame (TVF), the S-shaped duct located between the High-Pressure Turbine and the Low-Pressure Turbine, more difficult. The main benefit that the TVF offers is the reduction of the engine length, and therefore the reduction of its weight. The challenge in the design of the TVF is the fulfillment of both mechanical and aerodynamical requirements: on one hand, the TVF must provide mechanical support to the outer casing of the engine. On the other hand, the TVF must guide the flow to an increasing radius while at the same time providing flow turning with very low-aspect-ratio blades. Attempts were made in the literature to improve the performance of the TVF. However, the full design space was never fully exploited. For instance, the blades were optimized separately from the endwalls. In this paper, the TVF is optimized including the main strut, two splitter blades, and the hub and shroud endwalls. The total number of degrees of freedom is around 300 which led to a 30% loss reduction. Given the high number of degrees of freedom, a gradient-based optimization framework that allows tackling large design spaces thanks to the adjoint method is employed.

The comparison between the optimized geometry and the baseline highlighted some trends. The optimal endwall presents first a concave and then a convex shape in the bladed region. This promotes deceleration in the boundary layer at the leading edge and acceleration at the trailing edge. The initial deceleration allows for a reduction in the losses due to secondary flows, whereas the final acceleration prevents flow separation. Additionally, blade bowing can provide a further deceleration at the leading edge of the blade, enhancing the effect of the concave endwall. Finally, rear and uniform blade loading seems to be optimal, because it reduces flow deceleration on the suction side near the end of the blade.

KEYWORDS

Turbine Vane Frame, CFD, Gradient-Based, Adjoint, Optimization

NOMENCLATURE

Letter

C_{ax}	axial chord
J	objective function
L	angular momentum
m	mass
P_0	total pressure
R	radius
t	thickness
u	tangential direction
X_g	computational grid
Δ_{out}	Trailing Edge position
β	metal angle

δ	flow angle
ϕ	trailing edge angle
σ	Solidity

Abbreviation

<i>TVF</i>	Turbine Vane Frame
<i>LPT</i>	Low-Pressure Turbine
<i>HPT</i>	High-Pressure Turbine
<i>CFD</i>	Computational Fluid Dynamics
<i>RANS</i>	Reynolds Averaged Navier-Stokes
<i>SQP</i>	Sequential Quadratic Programming

INTRODUCTION

Higher efficiencies of modern aircraft engines have been mainly achieved by increasing the bypass ratio (Göttlich 2009). This trend has led to a steady increase in the radial dimension of the engine and introduced several challenges in the design of its components. One of the introduced challenges is the design of the Turbine Vane Frame. The primary purpose of the TVF is to guide the flow from the High-Pressure to the Low-Pressure Turbine, while simultaneously providing flow turning. The geometry of the TVF consists of an S-shaped duct, equipped with low-aspect-ratio blades which provide access to oil, cooling air supply lines, and mechanical support for the outer casing of the machine. These blades are called struts. In order to provide the necessary flow turning for the Low-Pressure Turbine, splitter blades are also present. Fig. 1 shows a typical turbine vane frame.

The main benefit offered by this multi-purpose component is the reduction in the axial length of the engine, which results in the reduction of its weight (Marn et al. 2009). The main challenge of this component lies in the complex interaction between its elements. The structural vane is sensitive to the negative incidence and it causes blockage, worsening the circumferential nonuniformity of the splitters (Lavagnoli et al. 2011). Additionally, strong secondary flows are present due to the low aspect ratio of the blades (Norris and Dominy, 1997). Attempts have been made in the literature to optimize the geometry of the blades and the endwalls separately (Yang and Wu 2016). Additionally, Clark et al. (2017) proposed the optimization of the 3D, multi-splitter configuration where each blade is parametrized using 6 degrees of freedom along three main sections. This is however in contrast with Masterts et al. (2017), where the suggested number of degrees of freedom for each blade profile is between 50 and 90.

In order to exploit further performance improvements, the optimization presented in this paper considers both endwalls and blades simultaneously, resulting in a total of 300 design parameters. To cope effectively with 300 design variables, a gradient-based adjoint method is

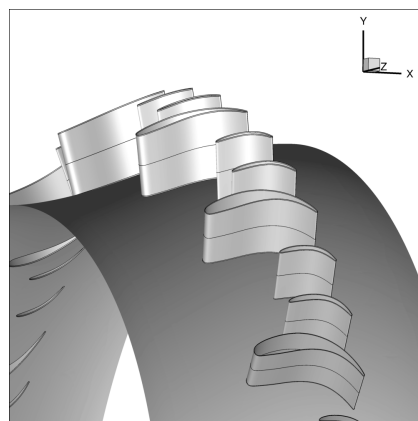


Figure 1: Geometry of the turbine vane frame

employed (Giles 2000). This paper is structured as follows: first, the optimization framework is briefly described, including geometry parametrization, meshing, as well as flow and adjoint solvers. Then, we describe the optimization problem and discuss the results by comparing the optimized TVF against the baseline geometry.

METHODOLOGY

Fig. 2 summarizes the optimization methodology: from an initial set of degrees of freedom α_0 , the geometry of the TVF is constructed. Then the elliptic grid generation constructs the mesh X_g and the CFD solver calculates the performance J . The Adjoint solver then solves the inverse problem and the gradient $\frac{dJ}{dU}$ is provided to the Sequential Quadratic Programming optimizer. The SQP optimizer provides a direction for the minimization of the objective and performs a non-derivative line search to ensure the respect of the Wolfe conditions (Wolfe, 1969). Once a suitable update for the design variables is obtained, the next major iteration restarts again from the geometry generation, closing the optimization loop. The optimization is terminated when both the update in the objective function and the L_2 norm of the gradient are below a pre-defined tolerance. Every step of Fig. 2 is performed with in-house software.

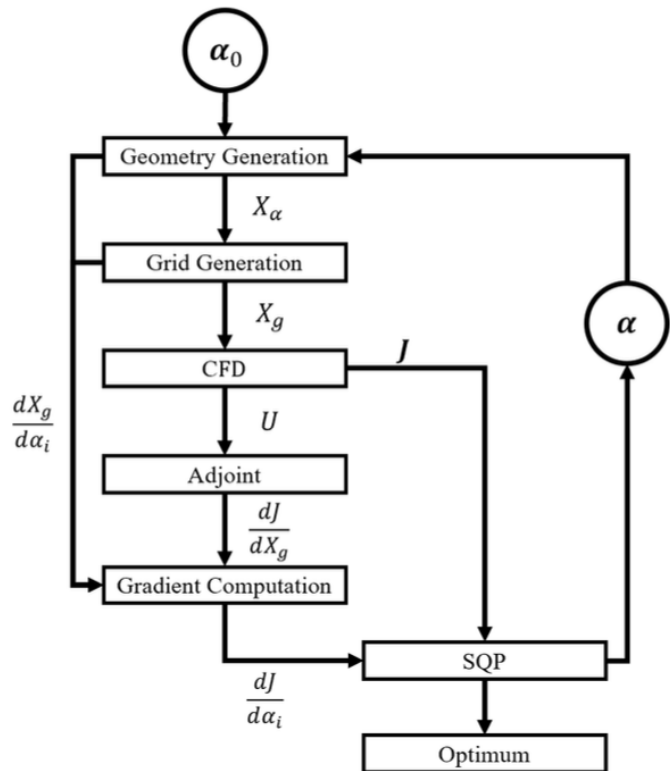


Figure 2: Optimization procedure

Parametrization and design variables

In the present paper, Bezier curves are used to parametrize the geometry of the blades and of the endwalls. The number of design parameters is 294, 24 of which are for the hub and shroud, 85 for each splitter, and 100 for the strut. The chosen parametrization provides high coverage of the design space, in line with Masters et al. (2017). The rationale is divided into two main parts: the 2D blade definition and the meridional definition. The 2D blade definition starts from the camber line and thickness distribution, as presented in Fig. 3. Firstly, the inlet metal angle β_{in} , outlet metal angle β_{out} , and stagger angle γ are defined. The value of the axial chord C_{ax} is set, and then the camber line is completely determined (Fig. 3, right). Then, to generate the pressure-side and suction-side curves, bezier control points are offset perpendicular to the camber line and this constitutes both curves. For the leading edge of the blade, the radius of curvature is set and this is translated into a constraint for the first two control points of the pressure side and suction side curves. The trailing edge of the blade is approximated as a semicircle and the connection with the pressure and suction side curves is controlled by the

trailing edge wedge angles ϕ_{SS} and ϕ_{PS} . Finally, the spacing to the adjacent blade is defined by the pitch.

In order to guarantee the continuity of the blade in the radial direction, the parameters that control the 2D blade profiles are defined by a continuous function that spans from hub to shroud. For example, the trailing edge position Δ_{out} at a particular radius r is obtained by the continuous function $\Delta_{out}(r)$. The advantage of this representation is that the blade is defined in every radial position with continuous curvature. Therefore, there is no need to use a shape space to ensure continuous curvature as in Clark et al. (2016). The control points of $\Delta_{out}(r)$ are the degrees of freedom of the optimization problem.

The connection between the 2D blade profiles and the 3D blade is performed via transfinite interpolation. After defining the hub and shroud curves according to Fig. 4, a series of surfaces spanning from hub to shroud is defined (Fig. 5). The 2D blade profile defined at the specific radius of the aforementioned surface is first selected and then interpolated from the 2D space onto the 3D surface. This layer-by-layer deposition of 2D blades provides the final shape of the 3D blade. The initial blades were obtained by extruding a previous 2D optimization (Orsenigo 2019) and the baseline endwalls were taken from the European project TATEF2 (Olive 2008).

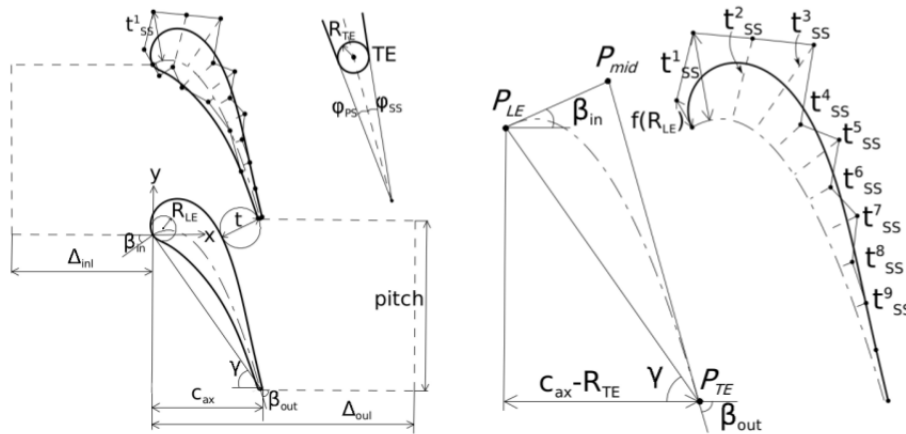


Figure 3: Geometrical parametrization of 2D blades

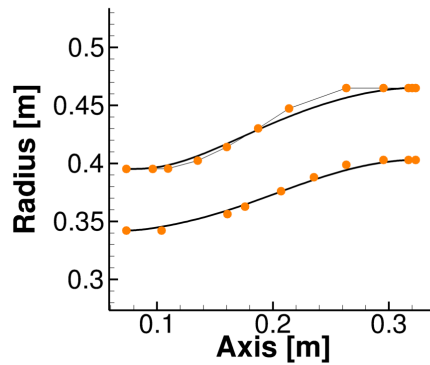


Figure 4: Hub and shroud curves with control points

Objective and Constraints

The objective is to minimize the total pressure loss coefficient J at design point:

$$J = \frac{P_{0,in} - P_{0,out}}{P_{0,in} - P_{out}} \quad (1)$$

where $P_{0,in}$, $P_{0,out}$, and P_{out} are respectively the total inlet pressure, total outlet pressure, and static outlet pressure.

The outlet flow angle δ_{out} is constrained to be the same as the baseline one $\delta_{out,design}$. This is achieved by imposing the design outlet flow angle as the minimum value for the outlet flow angle:

$$1 - \frac{\delta_{out}}{\delta_{out,design}} \leq 0 \quad (2)$$

This inequality constraint keeps the outlet flow angle as close as possible to the baseline one.

Finally, having good flow uniformity is important for the LPT after the TVF. This requirement is implemented in a simplified way: the outlet metal angle β_{out} of the strut and of the splitter, despite being variable, must be the same among the three blades.

$$\beta_{out,strut} = \beta_{out,splitter1} = \beta_{out,splitter2} \quad (3)$$

Grid generation

A multiblock structured grid with a total of 1.2 million cells is generated using an elliptic grid generator. A prior mesh convergence study was performed and the chosen cell count is the following: the splitters contain 300,000 cells and the strut 600,000 cells. The first cell height was set to achieve a value of $y^+ \sim 1$. The 3D mesh is generated using the layering technique: the 2D elliptic mesh generator solves the elliptic equations of Steger and Sorenson (1979) and creates a 2D mesh. Then the 2D meshes are layered in the radial direction and this creates the 3D mesh. The mesh generator allows for automatic code differentiation with the complex-step approach (Martins et al. 2003). This allows calculating $\frac{dX_g}{d\alpha}$, the sensitivity of the grid with respect to the design variables (Eqn. 4), in an automatic way. The flow sensitivity $\frac{dJ}{dX_g}$ is calculated from the adjoint variable, and then the gradient $\frac{dJ}{d\alpha}$ is computed by using the chain rule as follows:

$$\frac{dJ}{d\alpha} = \frac{dJ}{dX_g} \frac{dX_g}{d\alpha} \quad (4)$$

CFD and Adjoint solvers

The evaluation of the performance was carried out by solving the compressible Reynolds Averaged Navier-Stokes (RANS) equations with an in-house solver (Mueller 2019). Spatial discretization employs a cell-centered finite volume on multiblock structured grids. The perfect gas assumption was made, and the Spalart Allmaras turbulence model was selected for the turbulence problem closure. Solid walls were

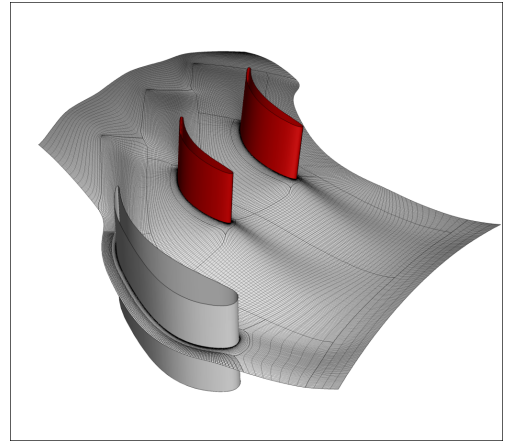


Figure 5: 3D grid generation by layering 2D grids

considered adiabatic. At the inlet of the computational domain, the total pressure, total temperature, and flow angle profiles were imposed. At the outlet, the pressure was prescribed with a correction accounting for radial equilibrium. The discrete adjoint technique was used for the calculation of the flow sensitivities. The flow sensitivities were solved with an adjoint code, which has been validated against complex-step gradients (Mueller 2019).

RESULTS

Fig. 6 shows the evolution of the normalized objective function and the outlet flow angle constraint. The optimization converged in 17 iterations and no further improvement of the objective could be found by the algorithm while satisfying the imposed constraint. The achieved reduction in the pressure loss coefficient is roughly 30 %.

Fig. 7 (a) and (b) compare the losses of the baseline and the optimized geometry at a plane located 30% axial chord downstream of the blade row. The entropy production of the optimized case is lower than the one of the original geometry. In particular, the core of the losses in the hub region significantly decreased. In order to investigate the main sources of loss generation, we discuss the geometric modifications of the optimized geometry and their impact on the flow field in the following sections.

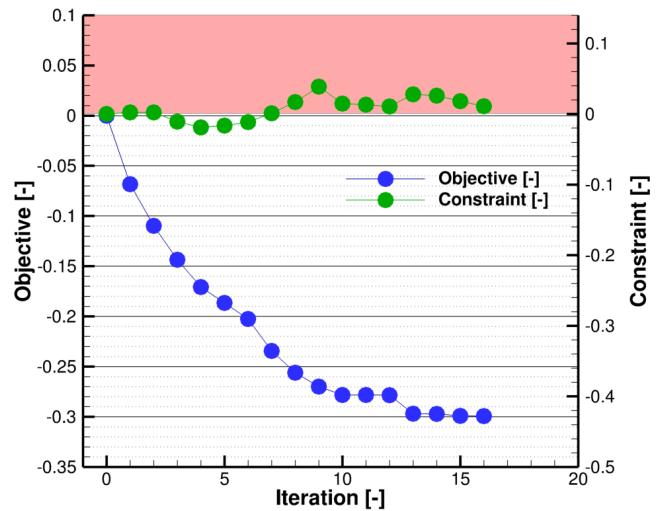


Figure 6: History of objective and constraint

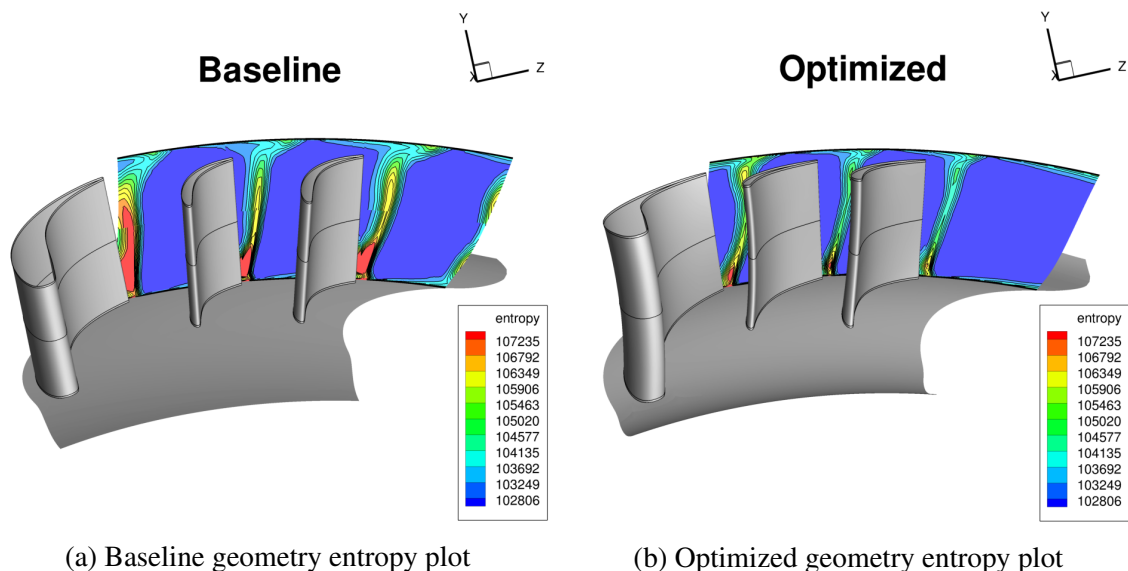
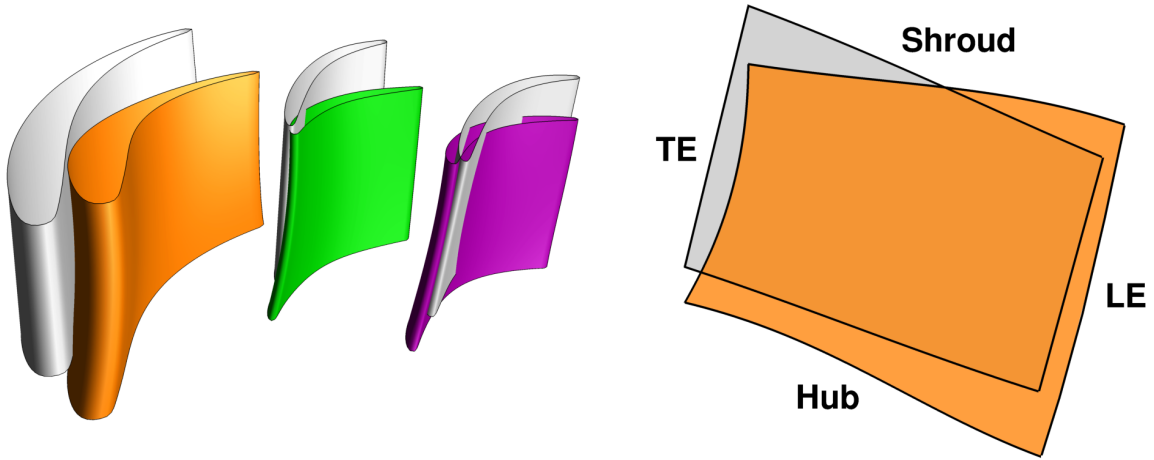


Figure 7: Loss contour 0.3 axial chords downstream the blade row

Geometry analysis

Fig. 8a compares the baseline and optimized blade profiles. Blade bowing was applied to the optimized TVF geometry and this reduced the losses by increasing the mass-flow rate passing in the center of the channel. This is in line with Wang et al. (1993), who show how positive bowing decreases the overall total pressure loss coefficient. Fig. 8b shows the optimized strut in the meridional plane. The optimized channel is concave at the leading edge of the blade and convex near the trailing edge. According to potential flow theory, the flow around a concave wall has a velocity gradient such that the velocity increases perpendicularly away from the wall. This results in a reduced velocity in the endwall region at the leading edge of the blade and, as will be discussed later, it reduces the secondary losses. Conversely, the convex end wall near the trailing edge promotes a higher velocity toward the wall, and thus acceleration occurs near the endwall at the trailing edge. This acceleration, as it will be further described later, prevents flow separation.

The optimal chord is reduced at midspan compared to the endwalls in Fig 8b. The radial evolution of the optimal blade solidity ($\sigma = C_{ax}/pitch$) can be explained by considering two sources of losses: the profile losses and the secondary losses. At midspan, the high-momentum flow produces high-profile losses. Therefore, a profile with lower solidity is beneficial since it reduces friction losses. On the other hand, the low-momentum fluid in the endwall region is characterized by the presence of secondary flows. A profile with higher solidity is beneficial since it provides better control of the low-momentum fluid and avoids sudden deceleration that can trigger flow separation.



(a) Frontal view of strut in orange, splitter 1 in green, splitter 2 in violet
 (b) Main strut details: baseline in grey, optimized in orange

Figure 8: Comparison between initial (grey) and optimized (coloured) blades

Fig. 9 compares the blade profiles at the hub, midspan, and shroud. Splitter 1 (green) and splitter 2 (purple) of the optimized geometry present a stagger angle that increases towards the shroud. This result comes from the conservation of the angular momentum ($L = R \times mv$) around the axis of the machine. As the flow leaving the vane frame goes to a higher radius, the tangential momentum remains constant, ($r \cdot v_u = const$). In the optimized case, the radius at the trailing edge is lower, so as to maintain the same tangential velocity at the domain outlet, a larger tangential velocity v_u at the shroud trailing edge is required.

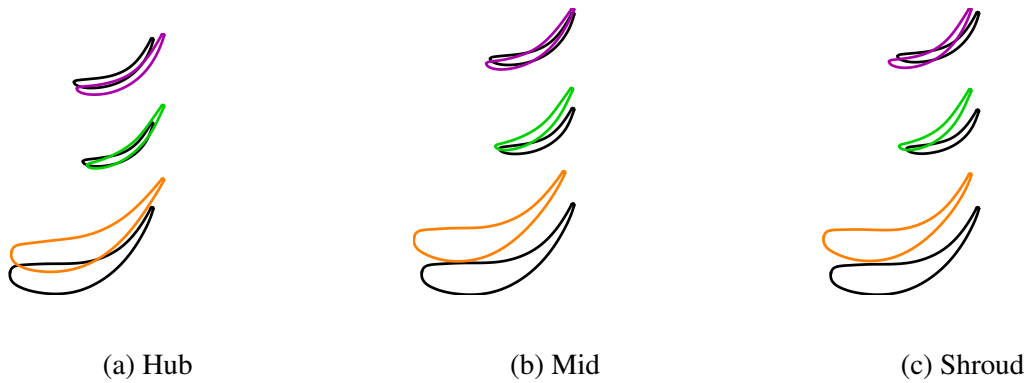


Figure 9: Blade profiles at hub, mid, and shroud. Baseline geometry in black. Optimized geometry: strut in orange, splitter 1 in green, splitter 2 in violet.

Profile losses

Fig. 10 represents the limiting streamlines obtained by projecting the stress tensor onto the blade surface and then performing integration. The flow direction is from right to left. The baseline geometry presents a region of flow separation near the trailing edge of the three blades. This flow separation is more pronounced in the shroud region where the flow has low momentum and the cross-sectional area of the component is increasing. The low-momentum fluid in the separation region is then pushed into the hub region by the radial pressure gradient due to the swirl of the flow. This is the main reason why in Fig. 7 most of the losses are concentrated in the hub region.

For the optimized geometry, on the other hand, the separation region is resolved, and all the limiting streamlines are flow-aligned.

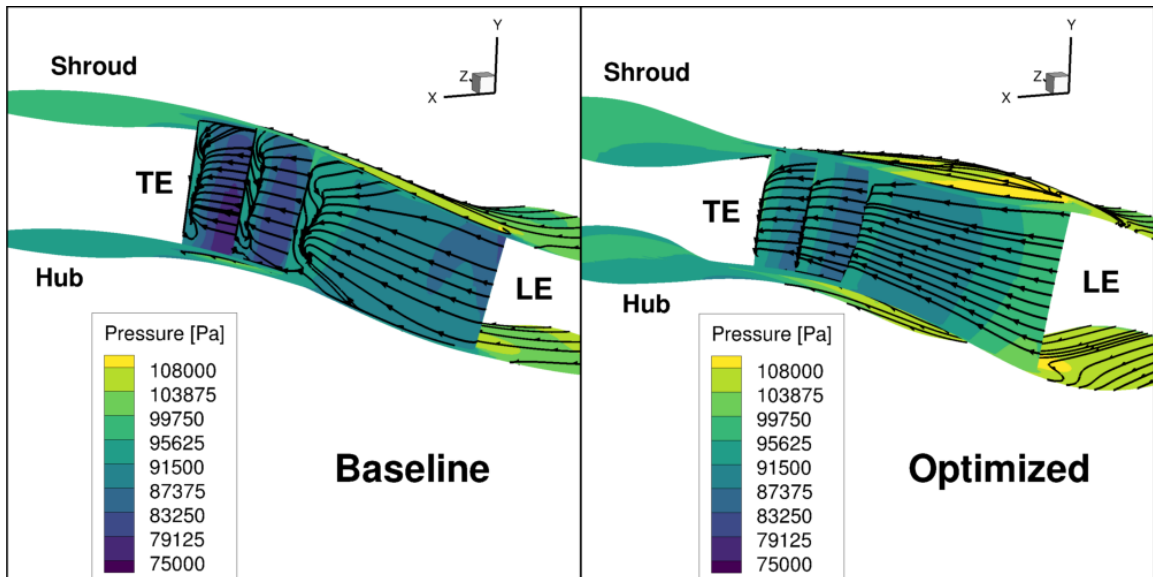


Figure 10: Comparison of blade limiting streamlines: baseline (left) and optimized (right)

Secondary flows

Secondary flows are another source of losses. Fig. 11 represents the limiting streamlines and the pressure contour at the hub and blades. In the baseline geometry, in the hub region next to the strut, the trace of the horseshoe vortices is visible. In the optimized case, the characteristic dimension of the horseshoe vortex changes significantly. In particular, the saddle point has moved more upstream compared to the baseline case and the characteristic velocity in the endwall region is smaller, thanks to the concave shape of the endwall. The higher dimension of the horseshoe vortex, associated with the smaller characteristic velocity in the endwall region suggests that the dissipation generated by the vortex core is smaller in the optimized case.

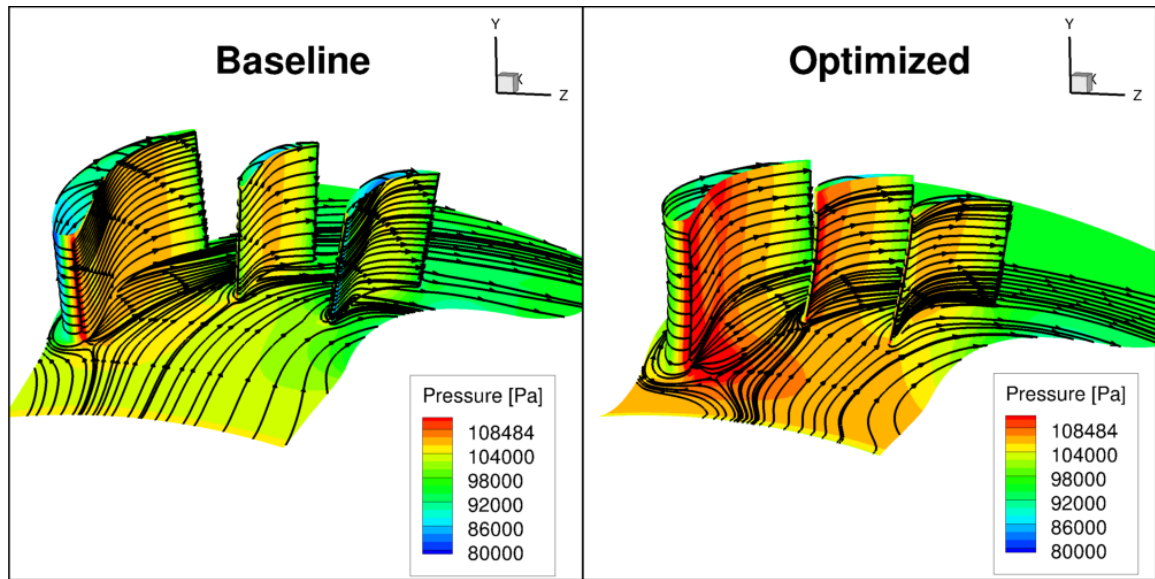


Figure 11: Comparison of hub limiting streamlines: baseline (left) and optimized (right)

Mass redistribution

Fig. 12 represents the distribution of the mass flow between the baseline and optimized cross-section in proximity to the leading edge of the main strut. The contour is the mass contribution of every cell normalized by the overall mass flow rate. The higher the value, the more mass flow rate goes through. More mass flow goes through the center of the channel in the optimized case compared to the baseline. This mass redistribution is beneficial since most of the losses are near the endwalls. By increasing the mass flow delivered to the center of the channel core, the amount of mass delivered toward the endwalls is reduced. This in turn reduces the overall, mass-averaged losses.

Blade loading

The load distribution on the blades is provided in Fig. 13. The isentropic Mach number is presented as a function of the dimensionless axial chord S/S_0 for midspan, close to the hub and close to the shroud. The baseline strut was front-loaded and this caused a rapid acceleration around the blade leading edge, followed by a deceleration towards the trailing edge. This was causing flow separation, especially in the proximity of the endwalls. Additionally, the isentropic Mach number in the proximity of the leading edge of baseline splitter 1 suggests a problem of negative incidence. Furthermore, the peak isentropic Mach number of splitter 1 is high and this forces a sudden diffusion towards the trailing edge of the blade.

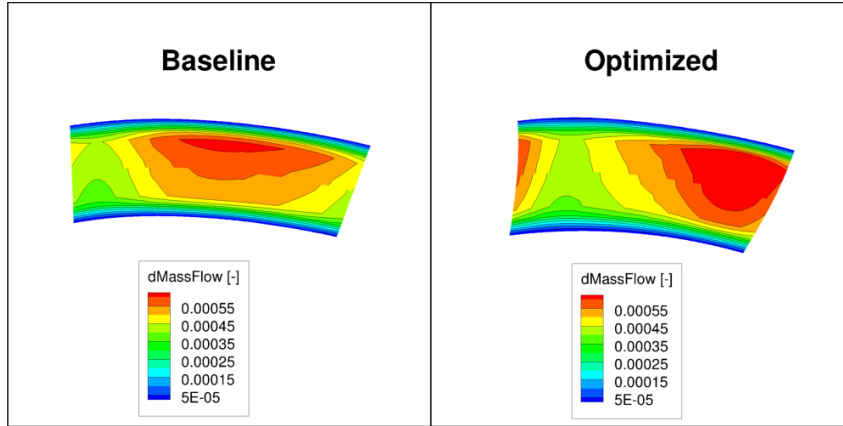


Figure 12: Mass flow rate distribution: baseline (left) and optimized (right)

In the optimized case, the strut is rear-loaded and this allows to avoid the flow deceleration that was characterizing the baseline geometry. Additionally, the Mach number peak at around 90% axial chord of splitter 1 is reduced and this results in a lower deceleration of the flow toward the trailing edge. Overall, the profile of the isentropic Mach number is more uniform in the optimized case, both along the radius and among the blades. This results in a more uniform load distribution and a consequent reduction in the losses.

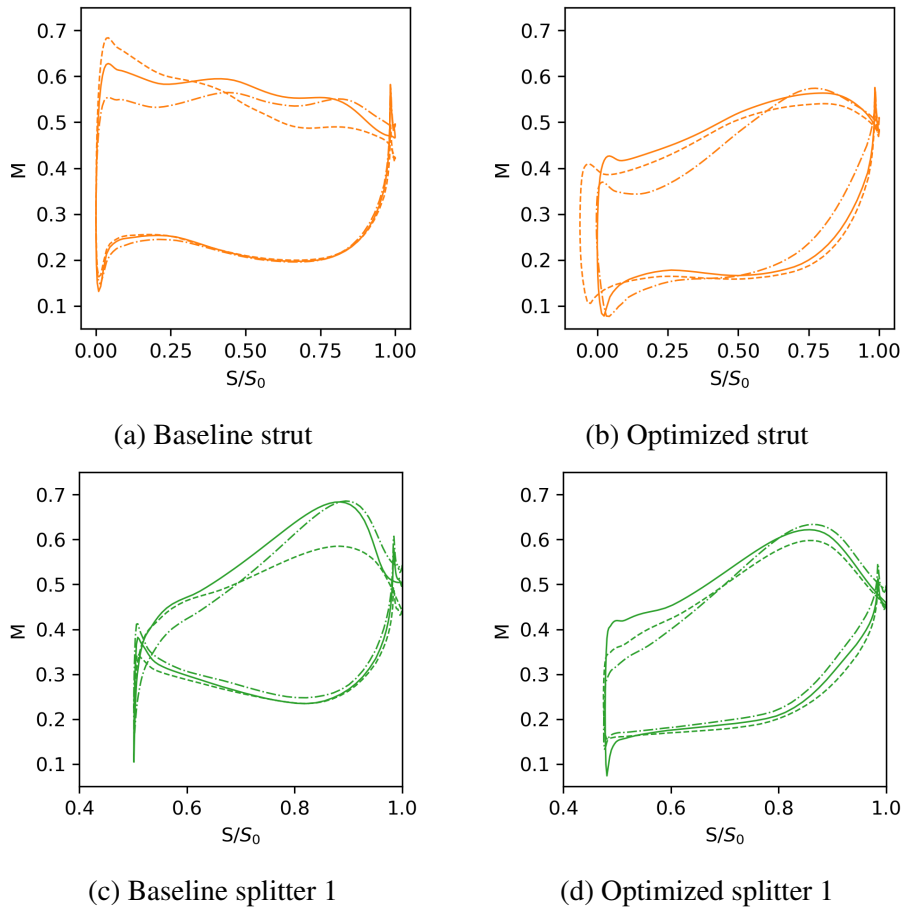


Figure 13: Blade isentropic Mach at midspan (filled), hub (dot-dashed) and shroud (dashed).

CONCLUSIONS

The present work investigated the aerodynamics of a 3D multi-splitter turbine vane frame equipped with structural load-bearing struts and splitter blades. The optimization of the component was successfully conducted using 294 design variables, including variable chord, thickness, lean, sweep, and endwall geometry. The optimization demonstrated the effectiveness of gradient-based optimization methods, as well as the importance of considering both blades and endwalls at the same time. The losses have been reduced by 30% at design operating conditions and the following observations have been made on the optimized geometry:

- The optimal endwall presents a concave and then convex shape in the proximity of the strut. This helps to reduce the losses due to secondary flows and to prevent flow separation at the trailing edge of the blades.
- The optimal strut exhibits a certain degree of bowing, which helps to further decrease the losses due to secondary flows.
- The optimal blades are rear-loaded which helps to avoid flow separation. Additionally, the maximum isentropic Mach number is the same for every blade and along the radius.

REFERENCES

- Bader, P., Sanz, W., Spataro, R., Göttlich, E., (2017). *Flow evolution through a turning mid turbine frame with embedded design*. Journal of Propulsion and Power, 33, 05, pp. 1 – 11.
- Chunqing T., Haisheng, C., Shinpei, M., Atsumasa, Y. (2003). *Influences of Blade Bowing on Flow-fields of Turbine Stator Cascades*. Aiaa Journal - AIAA J. 41. 1967-1972. 10.2514/2.1886.
- Clark, C. J., Pullan, G., Curtis, E., and Goenaga, F. (2017). *Secondary Flow Control in Low Aspect Ratio Vanes Using Splitters*. ASME. J. Turbomach. September 2017; 139(9): 091003
- Giles, M.B., Pierce, N.A. (2000). *An Introduction to the Adjoint Approach to Design*. Flow, Turbulence and Combustion 65, 393-415. <https://doi.org/10.1023/A:1011430410075>
- Marn, A., Göttlich, E., Cadrecha, D., Pirker, H. P. (2009). *Shorten the Intermediate Turbine Duct Length by Applying an Integrated Concept*. ASME. J. Turbomach. October 2009; 131(4): 041014. <https://doi.org/10.1115/1.3070578>
- Göttlich, E., (2011). *Research on the aerodynamics of intermediate turbine diffusers*. Progress in Aerospace Sciences, Volume 47, Issue 4. Pages 249-279, ISSN 0376-0421
- Lavagnoli, S., Yasa, T., Paniagua, G., Castillon, L., Duni, S. (2011). *Aerodynamic Analysis of an Innovative Low Pressure Vane Placed in an s-Shape Duct*. ASME. J. Turbomach. January 2012; 134(1): 011013. <https://doi.org/10.1115/1.4003241>
- Martins, J., Sturdza, P., Alonso, J., (2003). *The complex-step derivative approximation*. ACM Transactions on Mathematical Software, 29, pp.245 - 262. 10.1145/838250.838251. hal-01483287
- Masters, D.A., Taylor, N. J., Rendall, T. C. S., Allen, C. B. Poole D. J., (2017). *Geometric Comparison of Aerofoil Shape Parameterization Methods*. AIAA Journal 2017 55:5, 1575-1589
- Mueller L., (2019). *Adjoint-Based Optimization of Turbomachinery With Applications to Axial and Radial Turbines*. PhD Thesis, Université libre de Bruxelles, École polytechnique de Bruxelles, Bruxelles
- Norris G, Dominy RG. (1997). *Diffusion rate influences on inter-turbine diffusers*. Proceedings of the Institution of Mechanical Engineers, Part A: Journal of Power and Energy. 1997;211(3):235-242. doi:10.1243/0957650971537141
- Rémi Olive (2008). Technical report. *Final Report Summary - TATEF2 (Turbine Aero-Thermal External Flows 2)*. CORDIS EU research results. Available at <https://cordis.europa.eu/project/id/502924/reporting> [Verified 21 March 2023]

Russo, V., Orsenigo, S., Mueller, L., Verstraete, T. Lavagnoli, S.. (2019). *Adjoint Based Aerodynamic Optimization of a Multi-Splitter Turbine Vane Frame*. 10.1115/GT2019-91608.

Steger, J.L., Sorenson, R.L., (1979). *Automatic mesh-point clustering near a boundary in grid generation with elliptic partial differential equations*. Journal of Computational Physics, Volume 33, Issue 3, Pages 405-410, ISSN 0021-9991, [https://doi.org/10.1016/0021-9991\(79\)90165-7](https://doi.org/10.1016/0021-9991(79)90165-7). (<https://www.sciencedirect.com/science>)

Wolfe, P., (1969). *Convergence Conditions for Ascent Methods*. SIAM Review, vol. 11, no. 2, pp. 226-35. JSTOR, <http://www.jstor.org/stable/2028111>. Accessed 22 Mar. 2023.

Yang, C, Wu, H., (2016). *Optimized Aerodynamic Design of Aggressive Intermediate Turbine Duct With Strut Fairings Using Genetic Algorithms*. Proceedings of the ASME Turbo Expo 2016: Turbomachinery Technical Conference and Exposition. Volume 2A: Turbomachinery. Seoul, South Korea. June 13-17. V02AT40A004. ASME. <https://doi.org/10.1115/GT2016-56639>